Fast optical self-pulsing in a temporal analog of the Kerr-Slice pattern-forming system

G. Kozyreff,[1,2] T. Erneux,[1] M. Haelterman,[3] and P. Kockaert[3]

[1]*Optique Nonlinéaire Théorique, Université Libre de Bruxelles, Code Postal 231, Campus Plaine, B-1050 Bruxelles, Belgium*
[2]*ICFO—Institut de Ciencies Fotoniques, Mediterranean Technology Park, 08860 Castelldefels, Barcelona, Spain*
[3]*Service d'Optique et Acoustique, Université Libre de Bruxelles,*
Code Postal 194/5, avenue F.D. Roosevelt 50, B-1050 Bruxelles, Belgium

We present a double-pass optical loop containing a purely dispersive and an essentially purely nonlinear element as a potential fast intensity oscillator. The residual dispersion in the nonlinear element is found to play a key role in the dynamics. We analytically investigate the dynamics of the loop both for normal and anomalous dispersion, using linear and weakly nonlinear analysis. Numerically, stable operation is found for normal residual dispersion, while a tendency to multimode and irregular spiking is observed for anomalous dispersion. The effect of losses is also discussed.

I. INTRODUCTION

The control of optical dynamical instabilities is a useful way to generate pulse trains with high repetition rate out of continuous waves [1]. The modulation instability (MI) in optical fibers is a much studied example of this concept, partly because the pulses so obtained are close to optical solitons ([2], pp. 142–144). In particular, Nakazawa *et al.* [3] demonstrated fast intensity self-oscillations in a ring-cavity configuration. The latter, after subsequent improvements, evolved into what is now called the MI laser [4]. Meanwhile, other geometries involving counterpropagating waves [5,6] were also shown to spontaneously amplify perturbations and to play the role of oscillators. In all these configurations however, the repetition rate depends on the pump power and thus inherits its fluctuations.

In the same way as the temporal MI mentioned above results from the interplay between nonlinearity and group velocity dispersion, a number of spatial instabilities are produced by the coupling of nonlinearity with diffraction. One especially simple system supporting spatial MI is a thin Kerr-Slice with a feedback mirror [7–9] and many experimental setups function on this scheme. These have included liquid crystal light valves [10,11], nematic liquid crystal layers [12–14], or Na vapor cells [15,16] as nonlinear media. In particular, periodic [17] or quasicrystalline patterns [18] and "optical turbulence" [19] have been demonstrated. More recently, fractal patterns have been investigated [20]. We note for future reference that what limits the spatial frequency bandwidth is usually the diffusive character of the optical response of the Kerr element. This has motivated recent advances in the measurement techniques of this response [21].

In this paper, we analyze in detail a temporal analog of the Kerr-Slice with a feedback mirror that can be used as a fast oscillator. The choice of this particular system is motivated by the fact that, in the spatial case, the most unstable wave number is independent of the power. We expect the same for the natural frequency in the temporal case. In the usual Kerr-Slice experiment, an input wave passes through a nonlinear Kerr-Slice, diffracts in free space and is reflected by a mirror back to the Kerr-Slice [7]. By analogy, we consider a double-pass optical loop (Fig. 1) in which an input wave first passes through a nonlinear Kerr element, then disperses and passes a second time through the Kerr element. The basic idea underlying such a design is the following. In the nonlinear medium, the input wave undergoes a cross-phase modulation as it interacts with the wave that has already completed one roundtrip in the loop. Later on, due to the dispersive element between E and F in Fig. 1, this phase modulation becomes an *amplitude* modulation at the next roundtrip. This nonlinear feedback, as we will show, can lead to a modulation instability.

The analogy with the spatial system is complete if light passes only twice in the nonlinear medium. This is achieved by carefully controlling its polarization. If we temporarily ignore the nonlinear element in Fig. 1, then, with a suitable orientation of their axes, the two quarter-wave plates are equivalent to a single half-wave plate. They thus change an incoming *x*-polarized wave into a *y*-polarized wave. The two polarizing beam splitters PBS$_o$ and PBS$_i$ then perfectly reflect the wave, making it pass a second time through the two quarter-wave plates. After the second passage, the polariza-
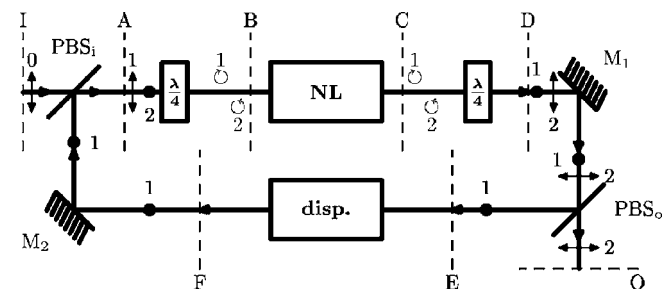
FIG. 1. The double-pass loop. Light enters through the polarizing beam splitter (PBS$_i$), passes twice in the nonlinear medium and leaves the loop through (PBS$_o$). The quarter-wave plates ($\lambda/4$) polarize the wave circularly in the nonlinear medium, with orthogonal polarizations in the first and in the second pass. They also globally rotate the linear input polarization by 90° between A and D, so that light is reflected by (PBS$_i$) in the first turn, and escapes the loop in the second one [see turn numbers next to the representations of the linear ($\updownarrow$, ●), and the circular ($\circlearrowleft$, $\circlearrowright$) polarization states].

tion is set back in the x direction and the wave leaves the system through PBS$_o$.

In the nonlinear element between the two quarter-wave plates, the linear states of polarization along the x and y directions become circular states, respectively $\mathbf{e}_+$ and $\mathbf{e}_-$, where $\mathbf{e}_\pm = (\mathbf{e}_x \pm i\mathbf{e}_y)/\sqrt{2}$. We assume that the nonlinear element is of the isotropic Kerr type, with Kerr coefficient γ, cross-phase modulation coefficient σ, and dispersion coefficient β_2^{NL}. In that case the slowly varying amplitudes $u_\pm$ of the two circular polarizations satisfy the vectorial nonlinear Schrödinger equation [22]

$$i\left(\frac{\partial}{\partial z} + \frac{1}{v}\frac{\partial}{\partial t}\right)u_\pm = \frac{\beta_2^{\mathrm{NL}}}{2}\frac{\partial^2 u_\pm}{\partial t^2} - \gamma(|u_\pm|^2 + \sigma|u_\mp|^2)u_\pm. \quad (1)$$

The coupling between the two waves u_+ and u_- only occurs through their intensities $|u_\pm|^2$ and is therefore incoherent. Moreover, there is no energy transfer between the two circular polarizations, hence it is still true that light makes two roundtrips in the loop. Note that incoherent coupling has also been achieved in cavities that are much longer than the coherence length of the signal [23].

It is worth emphasizing that the double-pass characteristic of the loop prevents us from assimilating the various sections inside the loop with a single element having average dispersion and nonlinearity coefficients. Indeed, a necessary condition for this would be that light cycled many times in it.

Before describing the full analysis of the system, a flavor of its dynamics can already be obtained from the simple following arguments. We assume that the nonlinear section is only weakly dispersive, i.e., that

$$\frac{\beta_2^{\mathrm{NL}}}{2}\frac{\partial^2 u_\pm}{\partial t^2} \ll \gamma|u_\pm|^2 u_\pm. \quad (2)$$

Hence it seems reasonable to neglect $\beta_2^{\mathrm{NL}}\partial^2 u_\pm/\partial t^2$ altogether. In this case, it has been shown [24] that the output power P_o evolves, in some properly rescaled time T, according to

$$P_o(T+\tau) = P_i|\mathcal{F}^{-1}[\mathcal{F}[e^{iP_o(T)/2P_c}]e^{2i\Omega^2}]|^2, \quad (3)$$

where P_i is the input power, $\mathcal{F}$ denotes Fourier transform, P_c is some critical power, τ is the rescaled loop roundtrip time, and Ω is the normalized frequency. In this equation $e^{2i\Omega^2}$ is a phase factor coming from the chromatic dispersion between sections E and F, while $e^{iP_o(T)/2P_c}$ stems from the cross-phase modulation in the nonlinear element between the u_+ and u_- waves.

In steady state, Eq. (3) admits the continuous wave (cw) solution $P_o(T) \equiv P_i$. On the other hand, according to the same equation, linear perturbations with frequency Ω are amplified at each roundtrip by a factor

$$G = -(P_i/P_c)\sin\Omega^2. \quad (4)$$

Hence, if $P_i > P_c$, the cw solution is unstable, with a maximum instability gain for all frequencies such that $|\sin\Omega^2| = 1$. This simplified model thus attests the existence of a modulation instability. However, the generation of arbitrary large frequencies is a physically unacceptable conclusion.

Actually, despite (2), dispersive effects cannot be entirely neglected in the nonlinear element. In the spatial case, these correspond to the small amount of diffraction taking place over the thickness of the thin Kerr-Slice, which is always neglected by comparison with the diffusive Kerr response. Here however, the Kerr response being assumed instantaneous, the dispersion or diffraction in the nonlinear element *is* the dominant bandwidth-limiting mechanism. Therefore, the existing linear stability results for the Kerr-Slice with feedback mirror are not transposable to the present system and we must reconsider the instability in the presence of this dispersion. This is what we do in the following section. We perform the analysis both in the linear and weakly nonlinear approximations. Particular attention is devoted to the effect of weak, anomalous, and finally to arbitrary dispersion. In Sec. III, we validate and extend our analytical findings by a series of numerical simulations. In particular, we discuss the effect of losses. Finally, we conclude by some further technical remarks on the experimental implementation of this system as well as some implications of the above results in the spatial domain.

In addition to the detailed stability analysis, the results described in this paper differ from those in [24] by the nonlinear bifurcation analysis, the study of the effect of anomalous dispersion, and the numerical simulations with or without losses that validate our analytical study. Finally, let us mention that some nanomechanical, Kerr-like systems (in which the optical path is a function of the light) are also found to produce power-independent pulsation under the action of a cw optical beam [25,26].

II. INSTABILITY

A. Preamble

We recall that the system under study has a finite size. The most natural way to address stability, therefore, is through a normal mode approach. We will thus consider small perturbations of the form

$$\delta\mathbf{u}(z,T) = \delta\hat{\mathbf{u}}(z)e^{-i\Omega T}, \quad (5)$$

where z is the longitudinal coordinate in the loop and T is time in appropriate units. For a normal mode to exist, Ω must satisfy some characteristic equation and is generally complex. Given an acceptable complex frequency $\Omega = \Omega' + i\Omega''$, Ω' is the actual oscillation frequency and Ω'' is the growth rate of the corresponding normal mode. Moreover, the amplification factor per roundtrip (of normalized duration τ) is given by $G = \exp(\Omega''\tau)$; our aim is thus to determine the relation between the gain per roundtrip (G) and the modulation frequency (Ω').

B. Model

Let β_2^{NL} and L_{NL} denote the dispersion coefficient and the length of the nonlinear section, respectively, and let β_2^D and L_D similarly characterize the dispersion section. Using the amplitude-phase decomposition $u = Ae^{i\phi}$, Eq. (1) becomes

$$\frac{\partial A_\pm}{\partial z} + \frac{1}{v_{\mathrm{NL}}}\frac{\partial A_\pm}{\partial t} = \beta_2^{\mathrm{NL}}\left(\frac{\partial A_\pm}{\partial t}\frac{\partial \phi_\pm}{\partial t} + \frac{A_\pm}{2}\frac{\partial^2 \phi_\pm}{\partial t^2}\right), \quad (6)$$

$$\frac{\partial \phi_{\pm}}{\partial z} + \frac{1}{v_{\mathrm{NL}}}\frac{\partial \phi_{\pm}}{\partial t} = \beta_2^{\mathrm{NL}}\left[\left(\frac{\partial \phi_{\pm}}{\partial t}\right)^2 - \frac{1}{2A_{\pm}}\frac{\partial^2 A_{\pm}}{\partial t^2}\right] + \gamma(A_{\pm}^2 + \sigma A_{\mp}^2). \tag{7}$$

Meanwhile, in the dispersive section, we have

$$\frac{\partial A_y}{\partial z} + \frac{1}{v_D}\frac{\partial A_y}{\partial t} = \beta_2^D\left(\frac{\partial A_y}{\partial t}\frac{\partial \phi_y}{\partial t} + \frac{A_y}{2}\frac{\partial^2 \phi_y}{\partial t^2}\right), \tag{8}$$

$$\frac{\partial \phi_y}{\partial z} + \frac{1}{v_D}\frac{\partial \phi_y}{\partial t} = \beta_2^D\left[\left(\frac{\partial \phi_y}{\partial t}\right)^2 - \frac{1}{2A_y}\frac{\partial^2 A_y}{\partial t^2}\right]. \tag{9}$$

To express the boundary conditions for these equations, let us write the vectorial amplitude of the electric field in a section ξ of Fig. 1 as

$$\mathbf{u}^{\xi} = u_x^{\xi}\mathbf{e}_x + u_y^{\xi}\mathbf{e}_y = u_+^{\xi}\mathbf{e}_+ + u_-^{\xi}\mathbf{e}_-. \tag{10}$$

We then have the following continuity relations:

$$\mathbf{u}^A(t + t_{FA}) = \sqrt{P_i}\mathbf{e}_x + u_y^F(t)\mathbf{e}_y, \tag{11}$$

$$\mathbf{u}^B(t + t_{AB}) = u_x^A(t)\mathbf{e}_+ + u_y^A(t)\mathbf{e}_-, \tag{12}$$

$$\mathbf{u}^D(t + t_{CD}) = u_-^C(t)\mathbf{e}_x + u_+^C(t)\mathbf{e}_y, \tag{13}$$

$$\mathbf{u}^E(t + t_{DE}) = u_y^D(t)\mathbf{e}_y, \tag{14}$$

$$\mathbf{u}^O(t + t_{DO}) = u_x^D(t)\mathbf{e}_x, \tag{15}$$

where P_i is the input power and $t_{\xi\xi'}$ is the time of flight between ξ and ξ'.

Setting $\partial/\partial t$ to zero everywhere, the only nontrivial part of the steady state $(A^s e^{i\phi^s})$ is in the nonlinear section. It is immediate from Eq. (6) that $\partial A_{\pm}^s/\partial z = 0$. Moreover, from the boundary conditions, $A_{\pm}^s = \sqrt{P_i}$. The phase equations (7) then imply that

$$\phi_{\pm}^s(z) = \phi_{\pm}^s(z_B) + \gamma P_i(1 + \sigma)(z - z_B) \tag{16}$$

in the nonlinear section.

C. Normal modes

We now study linear deviations from the steady state, of the form

$$A_{\alpha} = \sqrt{P_i}(1 + a_{\alpha}), \quad \phi_{\alpha} = \phi_{\alpha}^s + \varphi_{\alpha}, \tag{17}$$

α being any of the indices $\pm$, x, y. For convenience, we rescale time as

$$T = \sqrt{\frac{2}{\beta_2^D L_D}}t, \tag{18}$$

and, similarly, introduce T_{AB}, T_{BC},… as well as a nondimensional frequency Ω through $\Omega T = \omega t$. In the dispersive section, the normal modes take the following form

$$\begin{pmatrix} a_y \\ \varphi_y \end{pmatrix} = \begin{pmatrix} \hat{a}_y(z) \\ \hat{\varphi}_y(z) \end{pmatrix}e^{-i\Omega T}, \tag{19}$$

while in the nonlinear section of the loop, we have

$$\begin{pmatrix} a_+ \\ \varphi_+ \end{pmatrix} = \begin{pmatrix} \hat{a}_+(z) \\ \hat{\varphi}_+(z) \end{pmatrix}e^{-i\Omega T}. \tag{20}$$

Substituting in the evolution equations and using the boundary conditions, we then derive (see Appendix) the following relations:

$$\begin{pmatrix} \hat{a}_y \\ \hat{\varphi}_y \end{pmatrix}^F = e^{i\Omega T_{CF}}\mathbf{U}_D\begin{pmatrix} \hat{a}_+ \\ \hat{\varphi}_+ \end{pmatrix}^C, \tag{21}$$

$$\begin{pmatrix} \hat{a}_+ \\ \hat{\varphi}_+ \end{pmatrix}^C = e^{i\Omega T_{FC}}\mathbf{U}_{\mathrm{NL}}\begin{pmatrix} \hat{a}_y \\ \hat{\varphi}_y \end{pmatrix}^F, \tag{22}$$

where

$$\mathbf{U}_D = \begin{pmatrix} \cos \Omega^2 & -\sin \Omega^2 \\ \sin \Omega^2 & \cos \Omega^2 \end{pmatrix} \tag{23}$$

and

$$\mathbf{U}_{\mathrm{NL}} = \frac{1}{2}\begin{pmatrix} \cos \kappa_+\zeta_c - \cos \kappa_+\zeta_c & \dfrac{b \sin \kappa_-\zeta_c}{\kappa_-} - \dfrac{b \sin \kappa_+\zeta_c}{\kappa_+} \\ \dfrac{\kappa_+}{b}\sin \kappa_+\zeta_c - \dfrac{\kappa_-}{b}\sin \kappa_+\zeta_c & \cos \kappa_+\zeta_c - \cos \kappa_+\zeta_c \end{pmatrix}. \tag{24}$$

To shorten the notations, we have introduced above

$$\kappa_{\pm} = \sqrt{b(1 + b \pm \sigma)}, \tag{25}$$

where the parameter b measures the relative importance of dispersion and nonlinear phase modulation through the ratio

$$b = \frac{\beta_2^{\mathrm{NL}}\omega^2}{4\gamma P_i}. \tag{26}$$

The latter can also be expressed as $b = \beta'\Omega^2/2$, where $\beta' = \beta_2^{\mathrm{NL}}/(\gamma P_i \beta_2^D L_{\mathrm{NL}})$. Finally,

$$\zeta_c = 2\gamma P_i L_{\mathrm{NL}}. \tag{27}$$

Substituting expression (22) into (21), we obtain the characteristic equation

$$\det(\mathbf{I} - e^{i\Omega\tau}\mathbf{U}_D\mathbf{U}_{\text{NL}}) = 0, \quad \tau = T_{CF} + T_{FC}, \quad (28)$$

which allows us to analyze the stability of the constant output solution. As already explained in Sec. II A, each complex value of Ω that satisfies (28) defines a mode of frequency Ω', and growth rate Ω''. Computing the above determinant is a straightforward but rather tortuous exercise and leads to complicated expressions that are hard to interpret. We will therefore start our analysis of (28) by considering the limit $b \ll 1$, which is another way of expressing our basic assumption (2) that nonlinearity must dominate dispersion in the nonlinear element. Later on, we will compute solutions of (28) for arbitrary values of b and compare with our approximate theory.

1. Small dispersion limit

In the limit $b = \beta'\Omega^2/2 \to 0$, the characteristic equation (28) becomes

$$1 + \sigma\zeta_c e^{i\Omega\tau}\Big\{\sin\Omega^2 - \tfrac{1}{2}b\zeta_c\big[\zeta_c\sin\Omega^2\big(\sigma e^{i\Omega\tau}\cos\Omega^2 + \tfrac{2}{3}\big)$$
$$- \cos\Omega^2\big]\Big\} = O(b^2). \quad (29)$$

It can be further simplified by noting from above that $\sin\Omega^2 = -(\sigma\zeta_c e^{i\Omega\tau})^{-1} + O(b)$. Hence, to first order in b, Eq. (28) approximates as

$$1 + \tfrac{1}{3}b\zeta_c^2 + \sigma\zeta_c e^{i\Omega\tau}(\sin\Omega^2 + b\zeta_c\cos\Omega^2) = 0. \quad (30)$$

Bearing in mind that b is small, we thus identify $\sigma\zeta_c = 2\sigma\gamma P_i L_{\text{NL}}$ as a key group of parameters, which measures the system nonlinearity. This defines the critical power introduced in the model of Sec. I as

$$P_c = (2\sigma\gamma L_{\text{NL}})^{-1}. \quad (31)$$

The presence of σ confirms that the source of instability is cross-phase modulation, rather than self-phase modulation: if σ were zero then Eq. (30) could not be satisfied for any dynamical mode. Using $e^{i\Omega\tau} = e^{i\Omega'\tau}/G$, we can rearrange (30) slightly as

$$G\big(1 + \tfrac{1}{3}b\zeta_c^2\big) = -\sigma\zeta_c e^{i\Omega'\tau}(\sin\Omega^2 + b\zeta_c\cos\Omega^2). \quad (32)$$

The imaginary part of this equation

$$0 = \text{Im}\big[e^{i\Omega'\tau}\big(\sin\Omega^2 + \tfrac{1}{2}\beta'\Omega^2\zeta_c\cos\Omega^2\big)\big] \quad (33)$$

is a resonance condition for the frequency Ω. Coupled with the real part, it determines the spectrum of dynamical modes in the system. To make further progress, we now use the additional simplifying assumption of a long loop, in the sense that $\tau \gg 1$ or, dimensionally

$$t_{\text{cav}} \gg \sqrt{\beta_2^D L_D}, \quad (34)$$

t_{cav} being the dimensional loop roundtrip time. This condition is easily reached in fiber cavities. As a result, if

$$G \equiv e^{\Omega''\tau} = O(1), \quad (35)$$

then Ω'' is of order $1/\tau$. Hence $\Omega = \Omega' + O(1/\tau)$, and the resonance condition (33) is just
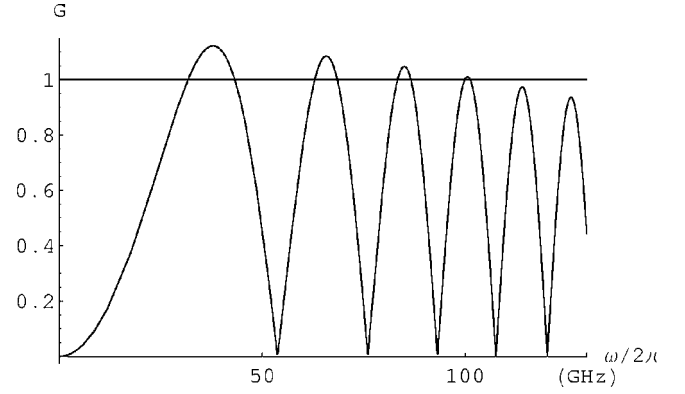
FIG. 2. Instability gain per roundtrip in the normal dispersion regime from the approximate formula (39). $P_i = 19$ mW, $\gamma = 1/(\text{W km})$, $\sigma = 2$, $L_{\text{NL}} = 15$ km, $L_D = 2.2$ km, $\beta_2^D = 25$ ps^2/km, $\beta_2^{\text{NL}} = 0.2$ ps^2/km. For this set of parameters, $b \simeq \omega/(2\pi 100 \text{ GHz})$.

$$e^{i\Omega'\tau} = \pm 1. \quad (36)$$

In fact, Ω' can vary quasicontinuously in this limit since any value of Ω' is $O(1/\tau)$ close to a resonant frequency. The gain per roundtrip, on the other hand, is now given by

$$G = \pm\sigma\zeta_c(\sin\Omega'^2 + b\zeta_c\cos\Omega'^2)\big(1 - \tfrac{1}{3}b\zeta_c^2\big). \quad (37)$$

By definition, G is positive and the sign above should be chosen accordingly. Since our aim is to determine instability thresholds, we restrict our attention to the maxima of G, i.e., to $|\sin\Omega'^2| = 1 - O(b)$ and therefore to $\cos\Omega'^2 = O(b^{1/2})$. Hence,

$$G = \pm\sigma\zeta_c\sin\Omega'^2\big(1 - \tfrac{1}{3}b\zeta_c^2\big) + O(b^{3/2}, 1/\tau)$$
$$= \pm\sigma\zeta_c\sin\Omega'^2\big(1 - \tfrac{1}{6}\beta'\zeta_c^2\Omega'^2\big), \quad (38)$$

or, dimensionally

$$G = \pm(P_i/P_c)\sin\big(\tfrac{1}{2}\beta_2^D L_D\omega'^2\big)\big(1 - \tfrac{1}{3}\gamma P_i\beta_2^{\text{NL}}L_{\text{NL}}^2\omega'^2\big). \quad (39)$$

This formula for the gain is illustrated in Fig. 2. Expression (38) with $b = 0$ is just the gain formula given in the preliminary model of the Introduction. For $P_i > P_c$, a quasicontinuous band of frequencies such that $P_c/P_i < |\sin(\Omega'^2)| < 1$ become unstable. Moreover, the instability gain has local maxima given by $\Omega' = \sqrt{(N+1/2)\pi}$, or

$$\omega' = \sqrt{\frac{(2N+1)\pi}{\beta_2^D L_D}}, \quad N = 0,1,2,\ldots. \quad (40)$$

Let us emphasize here that only $\beta_2^D L_D$ enters in the latter expression, not $\beta_2^D L_D + \beta_2^{\text{NL}}L_{\text{NL}}$. This is specifically due to the design of the loop, which is double pass and where the coupling is incoherent. Moreover, we note the interesting property that the maximum value of the instability gain only depends on the input power, while the associated frequency is solely determined by $\beta_2^D L_D$ and is thus stable against power fluctuations. This is not the case with other systems as, for instance, the MI laser [4,27].

Including the $O(b)$ correction, there is now a cut-off frequency, which can be found by setting $G=1$ and $|\sin(\frac{1}{2}\beta_2^D L_D \omega'^2)|=1$ in (39)

$$\omega_{\text{c.o.}}'^2 = \frac{12\sigma^2 \gamma P_c}{\beta_2^{\text{NL}}} \frac{P_c}{P_i}\left(1 - \frac{P_c}{P_i}\right). \quad (41)$$

For an order of magnitude estimate, let us notice that P_c and P_i are of the same order and hence, $\omega_{\text{c.o.}}' \sim \sqrt{\gamma P_i / \beta_2^{\text{NL}}}$.

2. Anomalous dispersion

The developments presented so far can also be done in the case of anomalous dispersion, i.e., if β_2^D or β_2^{NL} is negative. The results for anomalous dispersion in the dispersive section are easy to infer from the previous section. In this case, one should rescale time using $|\beta_2^D|$ and it is immediate to see that this leads to a minus sign in front of the second time derivative in Eq. (A2). As a result, all the formulas for the dispersive section can be obtained from the previous ones with the transformation $\Omega^2 \rightarrow -\Omega^2$. In particular, the gain formula (38) is still valid.

The treatment of the nonlinear section, on the other hand, involved b, which is proportional to β_2^{NL}. Hence, in the case of an anomalous dispersion in the nonlinear element, $b<0$ and Eq. (38) does not predict a finite bandwidth for the gain anymore. To remedy this problem, we must expand the characteristic polynomial to higher order in b. Here, we directly consider the large-delay limit. We obtain, after some manipulations

$$G \sim \sigma \zeta_c F\left[1 - \frac{1}{3}b\zeta_c^2 - \frac{1}{2}b^2\zeta_c^2\left(1 - \frac{3+\sigma^2}{60}\zeta_c^2\right)\right], \quad (42)$$

where

$$F = \sin \Omega'^2 + \left(b\zeta_c + \frac{1}{6}b^2\zeta_c^3\right)\cos \Omega'^2 + \frac{b^2\zeta_c^3\sigma}{12G}. \quad (43)$$

We thus see that the maxima of G, for which $\sin \Omega'^2 \simeq 1$ and $\cos \Omega'^2 \simeq 0$, now decrease for large values of $b = \beta'\Omega'^2/2$ and finite bandwidth is recovered. However, we do not expect the above formula to be quantitatively useful, since it is only valid for b small. Nevertheless, the form of the bandwidth-limiting factor in Eq. (42) suggests that anomalous dispersion allows larger bandwidth. This motivates us to solve the exact characteristic polynomial.

3. Arbitrary dispersion

We now compute the gain numerically for arbitrary values of b. Considering only the large-delay limit, the characteristic equation becomes, with $O(1/\tau)$ accuracy

$$\det(G\mathbf{I} - e^{i\Omega'}{}^\tau \mathbf{U}_D' \mathbf{U}_{\text{NL}}') = 0, \quad (44)$$

where $\mathbf{U}_D'$, $\mathbf{U}_{\text{NL}}'$ are obtained from $\mathbf{U}_D$, $\mathbf{U}_{\text{NL}}$ by replacing Ω with Ω'. Since in this limit Ω is essentially real, from now on, we will note Ω instead of Ω'.

Starting with the normal dispersion regime, we see by comparing Figs. 2 and 3 that the approximate formula accurately matches the exact curve in the limit $|b|\ll1$. On the
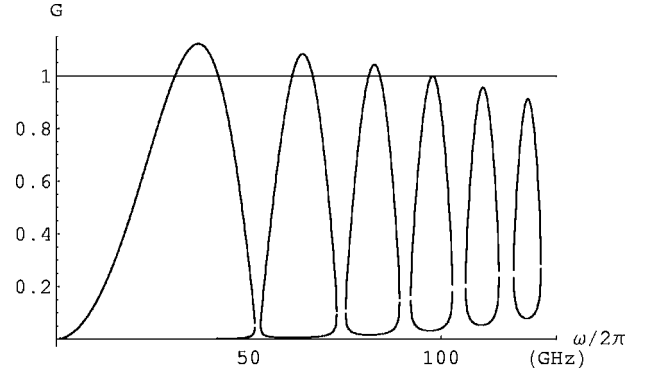
FIG. 3. Exact instability gain per roundtrip in the normal dispersion regime. Same parameter values as in Fig. 2.

other hand, the exact calculation reveals that the locus of dynamical modes in the (ω,G) plane is actually a set of closed curves. The effect becomes more and more pronounced for larger values of b, as illustrated in Fig. 4. There, formula (39) becomes less precise, although it still predicts reasonably well the position of the first gain maximum.

Finally, in Fig. 5, we plot the roundtrip gain in the anomalous dispersion regime. As anticipated, the maximum of the envelope of the gain is now shifted towards higher values of ω (see Fig. 5). Indeed, with the same absolute value of β_2^{NL} as in Figs. 2 and 3, the global maximum of G now appears at around ±150 GHz, instead of ±30 GHz in the normal case. The location of this maximum is now essentially determined by $b=O(1)$, hence by the balance between nonlinearity and dispersion in the nonlinear element, as in the classical modulation instability in optical fibers. This is at variance with the normal dispersion regime, where the first mode to become unstable has a frequency given by (40) with $N=1$. Moreover, Fig. 5 suggests that the anomalous regime more easily leads to multimode dynamics, where several lobes of frequency are simultaneously unstable. Hence, more complex dynamics can be expected beyond the instability threshold in that case.

D. Nonlinear analysis

A nonlinear analysis is possible if we consider a slightly revised version of the simplified model (3). Specifically, we
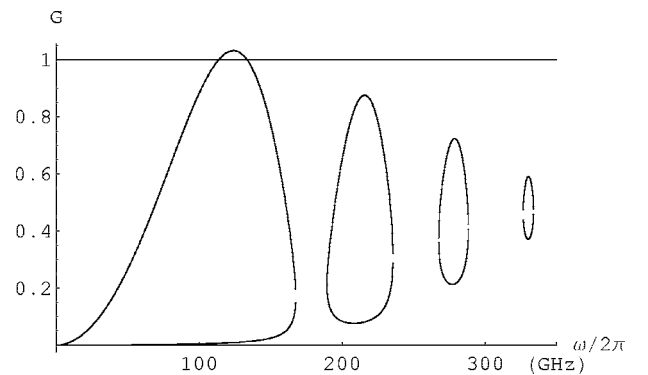
FIG. 4. Exact instability gain per roundtrip in the normal dispersion regime. $P_i=55$ mW, $\gamma=1/(\text{W km})$, $\sigma=2$, $L_{\text{NL}}=5$ km, $L_D=0.160$ km, $\beta_2^D=25$ ps^2/km, $\beta_2^{\text{NL}}=0.2$ ps^2/km.
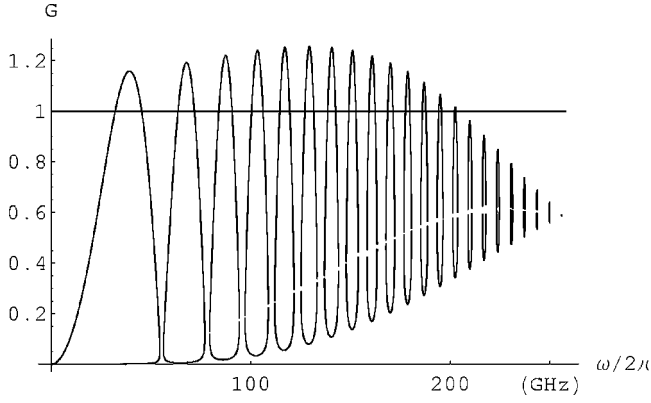
FIG. 5. Exact instability gain per roundtrip in the anomalous dispersion regime. $P_i = 21$ mW, $\gamma = 1/(\text{W km})$, $\sigma = 2$, $L_{NL} = 15$ km, $L_D = 2.2$ km, $\beta_2^D = 25$ ps^2/km, $\beta_2^{NL} = -0.2$ ps^2/km. For this set of parameters, $b \simeq -\omega/(2\pi 100 \text{ GHz})$.

investigate the bifurcation properties of the following equation:

$$P_o(T + \tau) = P_i |\mathcal{F}^{-1}[\mathcal{F}[e^{iP_o(T)/2P_c}]\mathcal{H}(\Omega)e^{2i\Omega^2}]|^2, \quad (45)$$

where, in the light of the preceding discussion, [Eq. (38)] we introduce a small dispersion in the nonlinear section by

$$\mathcal{H}(\Omega) = 1 - \tfrac{1}{6}\beta'\Omega^2\zeta_c^2. \quad (46)$$

Dealing with Eq. (45) rather than with the full model (6)–(9) considerably simplifies the algebra. The precise form of $\mathcal{H}$ is unimportant at this stage, as long as it only lets one mode destabilize at threshold. Note however that, due to this bandwidth-limiting factor, the threshold input power differs from P_c and we will denote it by P_{th}. We now construct a periodic solution of (45) of the form

$$P_i \sim P_{th}(1 + \epsilon^2 P_{i,2} + \cdots), \quad (47)$$

$$P_o \sim P_{th} + P_c(\epsilon \cos(\Omega T) + \epsilon^2 P_{o,2}(T) + \cdots), \quad (48)$$

where $\epsilon \ll 1$ is the oscillation amplitude close to threshold. The procedure for obtaining $P_{i,2}$ and $P_{o,2}(T)$ is a standard application of the Poincaré-Lindstet method and we omit the details for clarity. Substituting the above ansatz into Eq. (45) and expanding in power series of ϵ, we find at $O(\epsilon^2)$ that $P_{o,2}$ is constant and equal to $1/8$. Further, it emerges at $O(\epsilon^3)$ that the equation for the next correction $P_{o,3}(T)$ is only solvable if $P_{i,2} = 1/8$. Inserting this value in Eq. (47), we thus find that

$$\epsilon \sim \sqrt{8(P_i/P_{th} - 1)}. \quad (49)$$

Hence, the maxima of the output power are given by

$$P_{o,max} \sim P_{th} + \frac{1}{2\sigma\gamma L_{NL}}\sqrt{8(P_i/P_{th} - 1)}, \quad (50)$$

and the bifurcation is clearly supercritical $(P_i > P_{th})$. We compare this approximation with the exact numerical solution in the next section.

III. NUMERICAL STUDY

Having determined the instability thresholds, we now investigate the long-term evolution of the growing modes. To this end, instead of a true cw pumping, we simulate a synchronously pumped loop: at each roundtrip, a new pulse is injected, which is long enough (400 ps) to be considered as cw in its middle. In this way, we only need to discretize the vectorial nonlinear Schrödinger equation over a domain of several pulse widths in the moving frame, rather than over the whole loop in the case of true cw pumping. Moreover, this renders the boundary conditions (11)–(14) easier to implement and allows us to use efficient propagation algorithms, such as the split-step Fourier algorithm ([2], pp. 51–55).

A. Range of parameters

In our simulations, we use nonlinear coefficients and dispersion values that are typical of commercially available optical fibers. We also include the losses, since they are unavoidable in practice; these can strongly affect the dynamics of the system, as will be explained below.

The parameters used are chosen from (38) to ensure that only one mode can grow. To check robustness against noise, we added a random complex perturbation at the beginning of each turn into the loop. We found no significant changes with noise levels up to $10^{-2}P_i$ and the self-modulation profile was the same after 1000 and 10 000 roundtrips.

In a typical numerical simulation, the initial stage of the instability is accurately described by the linear stability analysis. The distribution of peaks in the power spectra faithfully reproduces that in the spectral gain curve derived in the previous sections, see Fig. 6(a). After this initial exponential growth, nonlinear effects set in and the first mode starts dominating the others. This can be viewed in Fig. 6(b), where the peaks are now equally spaced in the frequency domain and are all higher harmonics of the first one. Finally, the self-modulation amplitude saturates and reaches the state shown on Fig. 7. Note that even in this fully nonlinear regime, the self-modulation remains strongly sinusoidal. This is consistent with our weakly nonlinear analysis, which revealed that higher harmonics are absent at $O(\epsilon^2)$. We also plotted the maxima of $P_o(T)$ as a function of the input power P_i in Fig. 8 and found excellent agreement with the analytical approximation.

B. Distributed losses

We now study the effect of dissipation by including distributed losses in the simulations. To preserve the overall nonlinearity, these should be compensated, which can be done by either placing an amplifier in the loop or increasing the pump power. Both methods work but the latter is clearly preferable in view of keeping an experimental setup as simple as possible. The result of this compensation is shown in Fig. 9. From a series of simulations we reached the conclusion that the nonlinear section should be shorter than the absorption length. Otherwise, the power decreases significantly between sections B and C in Fig. 1. In extreme cases,
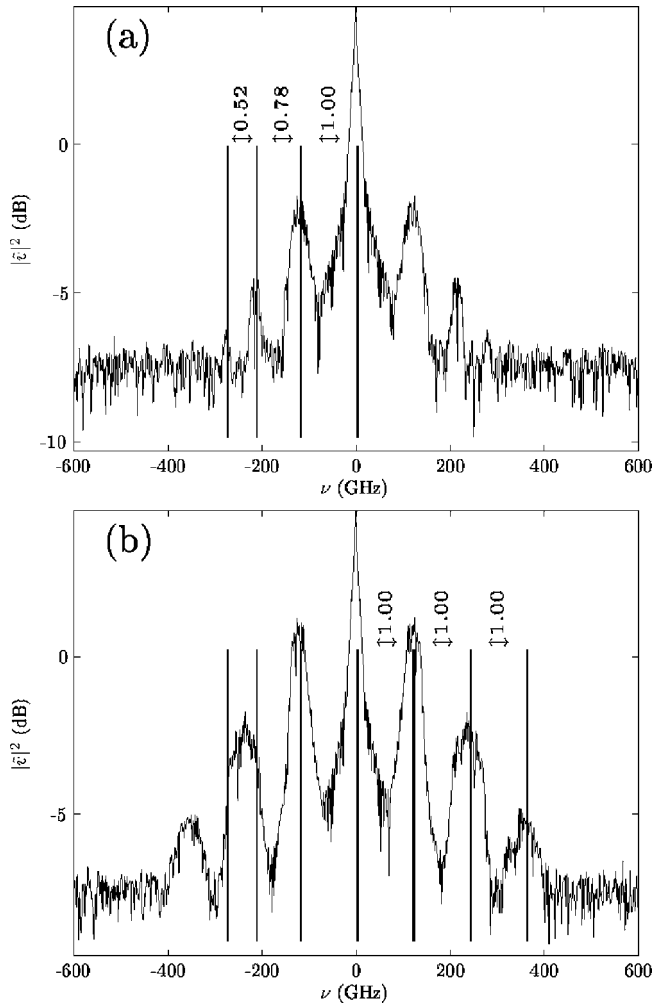
FIG. 6. Evolution of the unstable modes, after (a) 10, and (b) 20 roundtrips. The parameters are those of Fig. 4, except the input power, which is higher $P_i = 90$ mW in order to observe the growing of multiple modes. Vertical lines in the left of the two graphics, (a) and (b), show the positions of the growing modes in (a). These modes are not equally spaced. Their positions are predicted by (38), with less than 3% error. More precisely, the intermodal distances are in the ratio $(1, 1.78, 2.30)$; while theory predicts $(1, \sqrt{3}, \sqrt{5}) \approx (1, 1.73, 2.23)$. On the right side of the central peak in (b), vertical lines indicate the growing modes in (b). These lines are equally spaced, and do not follow (38).

one reaches the situation where nonlinear effects dominate close to B but become negligible compared to dispersion in C. In between the two, there is thus a region where nonlinearity and dispersion balance. This is comparable to the situation encountered with the MI laser [27], in which nonlinearity and dispersion act simultaneously everywhere in the cavity. Just as in the MI laser, then, when the pump power is increased, the self-pulsing dynamics quickly becomes irregular.

A typical loss figure is 0.2 dB/km. Hence, in our numerical simulations, we choose a 5-km-long nonlinear section.

C. Anomalous dispersion

The analysis presented in Sec. II C 2 showed that the dynamics of the modulation instability was strongly dependent
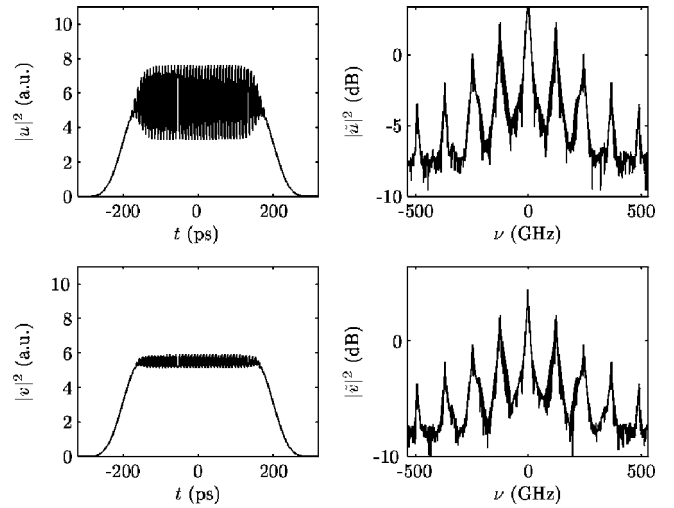
FIG. 7. Numerical simulations of the two orthogonally polarized slowly varying envelopes of the electric field, in the temporal domain (left) and in the spectral domain (right). Same parameters as in Fig. 4.

on the sign of the dispersion β_2^{NL}. Considering Fig. 5, we see that the mode with the highest gain does not correspond to the lowest MI frequency [$N > 1$ in (40)]. Moreover, the gain of the instability is almost the same for the main mode and those surrounding it. Therefore, we expect that the numerical simulations will reveal a complex dynamics, involving multiple modes, and that the monomode modulation instability will be observed only over a very limited range of input powers.

This is illustrated in Figs. 10 and 11 where the transition form cw [Figs. 10(a) and 11(a)] to multimode self-pulsing [Figs. 10(d) and 11(d)] occurs with an increase of the input power by less than one percent. In between, monomode self-pulsing can be found, but the instability gain is very small $(g - 1 \approx 10^{-2})$, so that saturation of the modulation is not yet attained after 8000 roundtrips in the loop, for the parameters of Figs. 10(b) and 10(c).
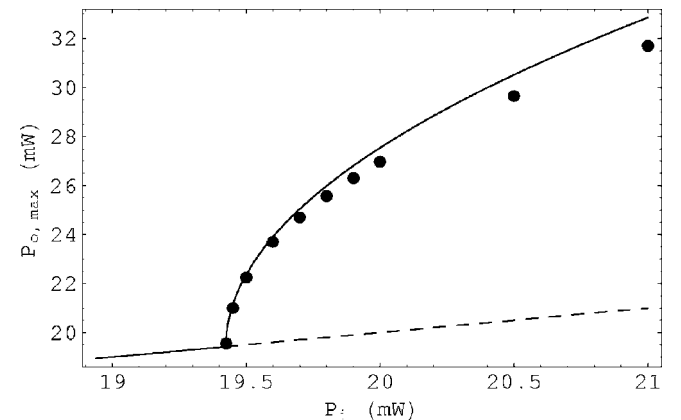
FIG. 8. Bifurcation diagram showing $P_{o,max}$ versus P_i with $\gamma = 1/(\text{W km})$, $\sigma = 2$, $L_{NL} = 15$ km, $L_D = 0.16$ km, $\beta_2^D = 25$ ps^2/km, $\beta_2^{NL} = 0.2$ ps^2/km. Full line: analytical approximation (50); dots: numerical simulation. For these parameter values the (exact) linear stability analysis yields the instability threshold $P_{th} = 19.424$ mW, the most unstable frequency being $\Omega/2\pi \simeq 100$ GHz.
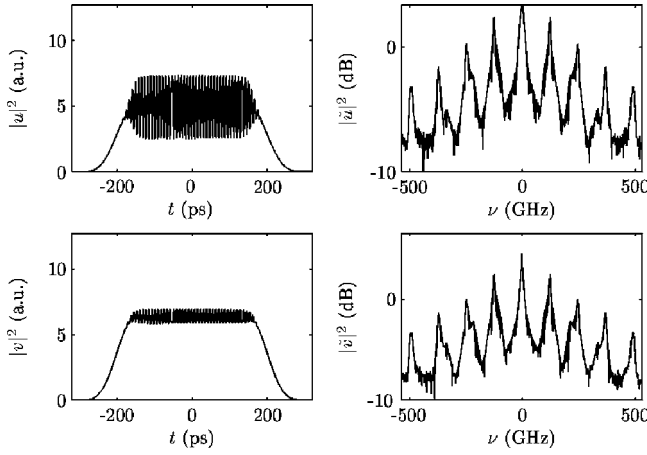
FIG. 9. Self-pulsing in the presence of 0.2 dB/km losses. Parameters are the same as in Figs. 4 and 7, but the input power P_i is raised to 88 mW.

In Sec. II C 2, we concluded that the gain formula (38) does not depend on the sign of the dispersion in the dispersive section (β_2^D). Numerically, this property is conserved when the losses and the nonlinearity in the dispersive section are include in the model. In particular, the numerical results presented in Figs. 10 and 11 were computed with $\beta_2^D < 0$. If we compare these results with those obtained when the sign of β_2^D is reversed, no significant changes are observed. However, the MI power threshold is slightly diminished (about 1%). This can be attributed to the additional scalar modulation instability that can develop in an anomalously dispersive section.

IV. CONCLUSION

In this paper, we have envisaged a temporal analog of the Kerr-Slice with feedback mirror as a way to generate trains
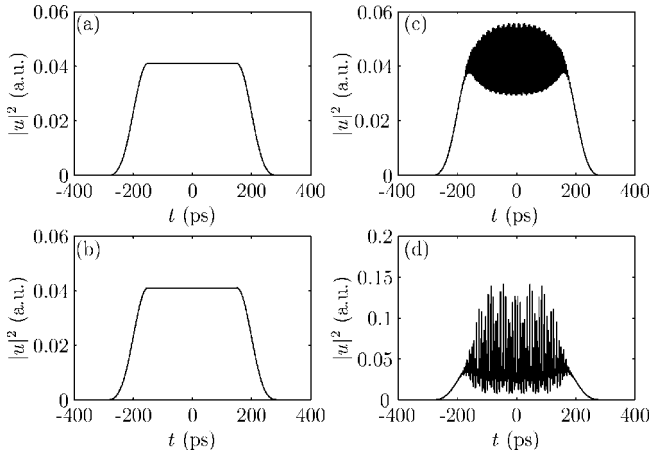
FIG. 10. Temporal output for different input powers after 8000 roundtrips. (a) $P_i = 65.40$ mW, (b) $P_i = 65.45$ mW, (c) $P_i = 65.85$ mW, (d) $P_i = 65.95$ mW. The other parameters are the same as those of Fig. 9, except that the signs of the dispersion coefficients are reversed: $\beta_2^{NL} = -0.2$ ps²/km, and $\beta_2^D = -25$ ps²/km. A variation less than one percent of the input power leads from the stable regime (a) to the multimode instability regime (d) (note the change of scale). As can be deduced from Fig. 5, there is a small range of input powers for which only one mode is growing.
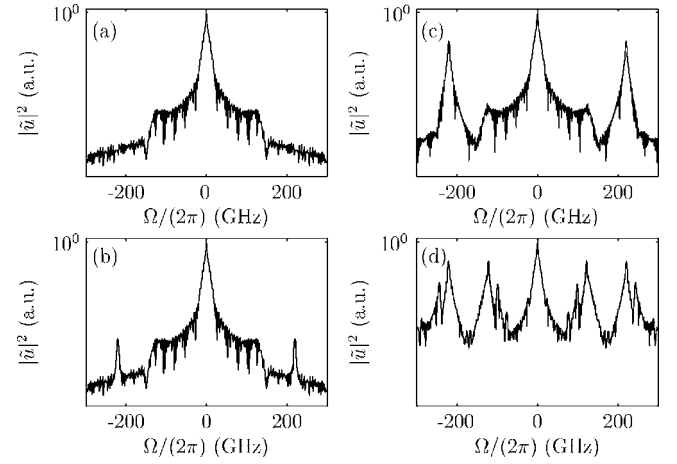
FIG. 11. Spectral intensities (in logarithmic scale) corresponding to the temporal intensities of Fig. 10. The input power is: (a) below instability threshold; (b) just above the instability threshold: two narrow modes are growing; (c) just below multimode threshold; (d) above multimode threshold. As expected from Fig. 5, additional modes are growing at lower and higher frequencies than the main mode.

of optical pulses. The scheme is promising for it allows us to reach frequencies on the order of 100 GHz with parameter values found in commercially available optical fibers. Of course, optical fibers are only taken as an example; other optical elements, such as photonic crystal fibers and gratings could equally be used. What eventually limits the bandwidth is the group velocity dispersion in the Kerr element, β_2^{NL}. In a practical experiment, one should work at optical frequencies close to the zero of this dispersion, meaning that both normal and anomalous dispersion would be experimentally accessible. From the linear stability analysis, the normal dispersion regime appears to be the most practical, because the global maximum of the gain is then given by $\omega = \sqrt{\pi/|\beta_2^D| L_D}$ and is thus independent of the input power. As in the spatial case, the result does not depend on the sign of β_2^D. Perhaps more surprising is the fact that it is also independent of $\beta_2^{NL} L_{NL}$. This results from the particular design of the optical loop as well as the incoherence of the nonlinear coupling between the two circularly polarized waves in the nonlinear element. If, on the other hand, β_2^{NL} is negative, then the global maximum of the instability gain is fixed by the balance between nonlinearity, γP_i, and the "nonlinear" dispersion, $\beta_2^{NL} \omega^2$, as in the classical MI in fibers. In that case, the oscillation frequency depends on the power and we lose the advantage of this setup with respect to others, such as the MI laser. In addition, we observed that this situation more easily leads to multimode dynamics. This is confirmed by our simulations, which clearly show a tendency to irregular spiking behavior in that case. By contrast, the self-pulsing in the normal dispersion regime is quite regular, and is neatly described by a weakly nonlinear analysis.

The incoherence of the coupling provides another technical advantage with respect to the MI laser: in the latter, the optical phase of the waves has to be precisely controlled, which imposes to maintain the cavity length constant down to optical wavelength precision. Here, on the other hand,

only the self-pulsing frequency comes into play. Therefore, in order to observe the dynamical modes, one should only stabilize the loop length down to the dynamical wavelength $2\pi v/\omega$, i.e., to a few mm. Another practical point worthy of consideration is the robustness of the scheme with respect to imperfectly polarized beams. Suppose for instance that the beam in section F of Fig. 1 is not orthogonally polarized with respect to the entrance beam but has undergone a parasitic rotation of $\pm 10°$. We checked numerically that with the polarizer PBS$_i$ having a standard 99% efficiency the dynamics remains qualitatively the same.

As we have pointed out, taking into account the effect of β_2^{NL} amounts, in the spatial analog, to treating the diffraction over the thickness of the Kerr-Slice. This with the difference, though, that the waves are counterpropagating in the Kerr-Slice. Nevertheless, it is by now clear that cut-off happens when dispersion or diffraction balances with nonlinearity. To be more specific, let us use Firth's notation [7] and parametrize the Kerr effect by χ [1/(W m)]. The role of β_2^{NL} is now played by the inverse optical wave number $1/k_0$. Hence, the expression $\omega_{\mathrm{c.o.}} \sim \sqrt{\gamma P_i/\beta_2^{\mathrm{NL}}}$ translates into $K_{\mathrm{c.o.}} \sim \sqrt{\chi k_0 P_i}$ for the cut-off spatial wave number and we note that it does not depend on the thickness of the slice. While this is a negligible effect in normal circumstances, it represents another limit to the size of fractal patterns predicted in [20], somewhere in between the optical wavelength and the diffusion length.

APPENDIX: DERIVATION OF THE NORMAL MODES

We start by writing the linear evolution equations for the perturbations in (17) in suitable time and space units. Having already introduced a nondimensional time T in (18), we still have to rescale the space variable. This can be done differently in the nonlinear and in the dispersive elements. In the latter, we define

$$Z = (z - z_E)/L_D, \tag{A1}$$

so that, with $V_D = v_D\sqrt{\beta_2^D/2L_D}$, the perturbations satisfy

$$\left(\frac{\partial}{\partial Z} + \frac{1}{V_D}\frac{\partial}{\partial T}\right)\begin{pmatrix} a_y \\ \varphi_y \end{pmatrix} = \frac{\partial^2}{\partial T^2}\begin{pmatrix} \varphi_y \\ -a_y \end{pmatrix}. \tag{A2}$$

In the nonlinear element, on the other hand, it is more convenient to use the rescaling

$$\zeta = 2\gamma P_i(z - z_B), \quad V_{\mathrm{NL}} = v_{\mathrm{NL}}\gamma P_i\sqrt{2\beta_2^D L_D}. \tag{A3}$$

This yields

$$\left(\frac{\partial}{\partial\zeta} + \frac{1}{V_{\mathrm{NL}}}\frac{\partial}{\partial T}\right)\begin{pmatrix} a_+ \\ \varphi_+ \\ a_- \\ \varphi_- \end{pmatrix} = \frac{\beta'}{2}\frac{\partial^2}{\partial T^2}\begin{pmatrix} \varphi_+ \\ -a_+ \\ \varphi_- \\ a_- \end{pmatrix} + \begin{pmatrix} 0 \\ a_+ + \sigma a_- \\ 0 \\ a_- + \sigma a_+ \end{pmatrix}, \tag{A4}$$

where

$$\beta' = \frac{\beta_2^{\mathrm{NL}}}{\gamma P_i\beta_2^D L_D}. \tag{A5}$$

From the continuity relations (11)–(14), we must solve Eq. (A2) in the domain $0 < Z < 1$ with the boundary conditions

$$a_y(Z = 0, T) = a_+(\zeta = \zeta_c, T - T_{CE}),$$

$$\varphi_y(Z = 0, T) = \varphi_+(\zeta = \zeta_c, T - T_{CE}), \tag{A6}$$

where $\zeta_c = 2\gamma P_i L_{\mathrm{NL}}$, and Eq. (A4) in the interval $0 < \zeta < \zeta_c$ with the boundary conditions

$$a_+(\zeta = 0, T) = 0,$$

$$\varphi_+(\zeta = 0, T) = 0,$$

$$a_-(\zeta = 0, T) = a_y(Z = 1, T - T_{FB}),$$

$$\varphi_-(\zeta = 0, T) = \varphi_y(Z = 1, T - T_{FB}). \tag{A7}$$

In order to construct the normal modes, we now look for solutions of Eq. (A2) of the form

$$\begin{pmatrix} a_y \\ \varphi_y \end{pmatrix} = \begin{pmatrix} \hat{a}_y(Z) \\ \hat{\varphi}_y(Z) \end{pmatrix}e^{-i\Omega T}. \tag{A8}$$

The vector amplitude $(\hat{a}_y(Z), \hat{\varphi}_y(Z))^T$ is generally a combination of exponentials $\exp(i\Omega Z/V_D + iKZ)$ with $K = \pm\Omega^2$, and we find that

$$\begin{pmatrix} \hat{a}_y \\ \hat{\varphi}_y \end{pmatrix} = \begin{pmatrix} c_1\cos(\Omega^2 Z) - c_2\sin(\Omega^2 Z) \\ c_1\sin(\Omega^2 Z) + c_2\cos(\Omega^2 Z) \end{pmatrix}e^{i(\Omega/V_D)Z}, \tag{A9}$$

where c_1 and c_2 are arbitrary constants. Similarly, in the nonlinear section of the loop, the solution of Eq. (A4) can be written as

$$\begin{pmatrix} a_+ \\ \varphi_+ \\ a_- \\ \varphi_- \end{pmatrix} = \begin{pmatrix} \hat{a}_+(\zeta) \\ \hat{\varphi}_+(\zeta) \\ \hat{a}_-(\zeta) \\ \hat{\varphi}_-(\zeta) \end{pmatrix}e^{-i\Omega T}. \tag{A10}$$

Here again, $(\hat{a}_+(\zeta), \hat{\varphi}_+(\zeta), \hat{a}_-(\zeta), \hat{\varphi}_-(\zeta))^T$ is a combination of exponentials $\mathbf{v}\exp(i\Omega\zeta/V_{\mathrm{NL}} + i\kappa\zeta)$, this time such that

$$\begin{pmatrix} i\kappa & b & 0 & 0 \\ -1-b & i\kappa & -\sigma & 0 \\ 0 & 0 & i\kappa & b \\ -\sigma & 0 & -1-b & i\kappa \end{pmatrix}\mathbf{v} = \mathbf{0}, \tag{A11}$$

where we have introduced

$$b = \frac{\beta' \Omega^2}{2} = \frac{\beta_2^{\mathrm{NL}} \omega^2}{4 \gamma P_i} \tag{A12}$$

to shorten the notations. The characteristic polynomial of Eq. (A11) is

$$\kappa^4 - 2b(1+b)\kappa^2 + b^2[(1+b^2) - \sigma^2] \tag{A13}$$

and has the four roots $\kappa = \pm \kappa_{\pm}$, where

$$\kappa_{\pm} = \sqrt{b(1 + b \pm \sigma)}. \tag{A14}$$

The eigenvectors associated to κ_{+}, $-\kappa_{+}$, κ_{-}, $-\kappa_{-}$ are $\mathbf{v}_1$, $\mathbf{v}_2$, $\mathbf{v}_3$, and $\mathbf{v}_4$, respectively, with

$$\mathbf{v}_1 = \left(1, \frac{\kappa_+}{ib}, 1, \frac{\kappa_+}{ib} \right)^T,$$

$$\mathbf{v}_2 = \left(1, -\frac{\kappa_+}{ib}, 1, -\frac{\kappa_+}{ib} \right)^T,$$

$$\mathbf{v}_3 = \left(-1, -\frac{\kappa_-}{ib}, 1, \frac{\kappa_-}{ib} \right)^T,$$

$$\mathbf{v}_4 = \left(-1, \frac{\kappa_-}{ib}, 1, -\frac{\kappa_-}{ib} \right)^T. \tag{A15}$$

Hence, the general solution of (A4) is

$$\begin{pmatrix} \hat{a}_+ \\ \hat{\varphi}_+ \\ \hat{a}_- \\ \hat{\varphi}_- \end{pmatrix} = (d_1 \mathbf{v}_1 e^{i\kappa_+ \zeta} + d_2 \mathbf{v}_2 e^{-i\kappa_+ \zeta} + d_3 \mathbf{v}_3 e^{i\kappa_- \zeta}$$

$$+ d_4 \mathbf{v}_4 e^{-i\kappa_- \zeta}) e^{i(\Omega/V_{\mathrm{NL}})\zeta}. \tag{A16}$$

Expressions (A9) and (A16) allow us to follow the evolution of a perturbation circulating in the loop. The constants of integrations $c_1, c_2, d_1, \ldots, d_4$ are obtained from the continuity conditions. On the one hand, from (A6), we find that c_1 and c_2 are just given by

$$\begin{pmatrix} c_1 \\ c_2 \end{pmatrix} = e^{i\Omega T_{CE}} \begin{pmatrix} \hat{a}_+ \\ \hat{\varphi}_+ \end{pmatrix}^C. \tag{A17}$$

This, with (A9) leads to Eq. (21). On the other hand, from (A7), we obtain

$$\begin{pmatrix} d_1 \\ d_2 \\ d_3 \\ d_4 \end{pmatrix} = \frac{e^{i\Omega T_{FB}}}{4} \begin{pmatrix} \hat{a}_y + ib\hat{\varphi}_y/\kappa_+ \\ \hat{a}_y - ib\hat{\varphi}_y/\kappa_+ \\ \hat{a}_y + ib\hat{\varphi}_y/\kappa_- \\ \hat{a}_y - ib\hat{\varphi}_y/\kappa_- \end{pmatrix}^F, \tag{A18}$$

which, with (A16), yields Eq. (22).

---

[1] S. L. McCall, Appl. Phys. Lett. **32**, 284 (1977).

[2] G. P. Agrawal, *Nonlinear Fiber Optics*, 3rd ed. (Academic Press, San Diego, California, 2001).

[3] M. Nakazawa, K. Suzuki, and H. A. Haus, Phys. Rev. A **38**, 5193 (1988).

[4] S. Coen and M. Haelterman, Phys. Rev. Lett. **79**, 4139 (1997).

[5] C. Law and A. Kaplan, Opt. Lett. **14**, 734 (1989).

[6] W. Firth and C. Penman, Opt. Commun. **94**, 183 (1992).

[7] W. Firth, J. Mod. Opt. **37**, 151 (1990).

[8] G. D'Alessandro and W. J. Firth, Phys. Rev. Lett. **66**, 2597 (1991).

[9] G. D'Alessandro and W. J. Firth, Phys. Rev. A **46**, 537 (1992).

[10] S. Akhmanov, M. Vorontsov, and V. Ivanov, JETP Lett. **47**, 707 (1988).

[11] B. Thüring, R. Neubecker, and T. Tschudi, Opt. Commun. **102**, 111 (1993).

[12] M. Tamburrini, M. Bonavita, S. Wabnitz, and E. Santamato, Opt. Lett. **18**, 855 (1993).

[13] F. Castaldo, D. Paparo, and E. Santamento, Opt. Commun. **143**, 57 (1997).

[14] E. Louvergneaux, C. Szwaj, G. Agez, P. Glorieux, and M. Taki, Phys. Rev. Lett. **92**, 043901 (2004).

[15] G. Giusifredi, J. Valley, R. Pon, G. Khitrova, and H. Gibbs, J. Opt. Soc. Am. B **5**, 1181 (1988).

[16] T. Ackemann and W. Lange, Phys. Rev. A **50**, R4468 (1994); http://link.aps.org/abstract/PRA/v50/pR4468

[17] R. Mcdonald and H. Eichler, Opt. Commun. **89**, 289 (1992).

[18] E. Pampaloni, P. L. Ramazza, S. Residori, and F. T. Arecchi, Phys. Rev. Lett. **74**, 258 (1995); http://link.aps.org/abstract/PRL/v74/p258

[19] S. A. Akhmanov, M. A. Vorontsov, V. Y. Ivanov, A. V. Larichev, and N. I. Zheleznykh, J. Opt. Soc. Am. B **9**, 78 (1992); http://josab.osa.org/abstract.cfm?id=6203

[20] J. G. Huang and G. S. McDonald, Phys. Rev. Lett. **94**, 174101 (2005).

[21] G. Agez, P. Glorieux, and E. Louvergneaux, Opt. Commun. **245**, 243 (2005).

[22] N. Akhmediev and A. Ankiewicz, *Solitons, Nonlinear Pulses and Beams* (Chapman and Hall, London, 1997).

[23] T. Carmon, M. Soljačić, and M. Segev., Phys. Rev. Lett. **89**, 183902 (2002).

[24] P. Kockaert, G. Kozyreff, C. Cambournac, M. Haelterman, and T. Erneux, Opt. Lett. **31**, 495 (2006).

[25] L. Sekaric, M. Zalalutdinov, S. W. Turner, A. T. Zehnder, J. M. Parpia, and H. G. Craighead, Appl. Phys. Lett. **80**, 3617 (2002).

[26] T. Carmon, H. Rokhsari, L. Yang, T. J. Kippenberg, and K. J. Vahala, Phys. Rev. Lett. **94**, 223902 (2005).

[27] S. Coen, M. Tlidi, Ph. Emplit, and M. Haelterman, Phys. Rev. Lett. **83**, 2328 (1999).